JMEPEG (2017) 26:5760–5768
https://doi.org/10.1007/s11665-017-3049-0

1059-9495/$19.00

Titanium Alloys Thin Sheet Welding with the Use of Concentrated Solar Energy

D.I. Pantelis, M. Kazasidis, and P.N. Karakizis

(Submitted May 26, 2017; in revised form August 1, 2017; published online November 1, 2017)

The present study deals with the welding of titanium alloys thin sheets 1.3 mm thick, with the use of concentrated solar energy. The experimental part of the work took place at a medium size solar furnace at the installation of the Centre National de la Recherche Scientifique, at Odeillo, in Southern France, where similar and dissimilar defect-free welds of titanium Grades 4 and 6 were achieved, in the butt joint configuration. After the determination of the appropriate welding conditions, the optimum welded structures were examined and characterized microstructurally, by means of light optical microscopy, scanning electron microscopy, and microhardness testing. In addition, test pieces extracted from the weldments were tested under uniaxial tensile loading aiming to the estimation of the strength and the ductility of the joint. The analysis of the experimental results and the recorded data led to the basic concluding remarks which demonstrate increased hardness distribution inside the fusion area and severe loss of ductility, but adequate yield and tensile strength of the welds.

Keywords concentrated solar energy, tensile properties, thin sheet, titanium, welding

1. Introduction

The use of concentrated solar energy (CSE) and power (CSP) technology is considered to be a reliable and promising alternative method of energy production (Ref 1-3) and material treatment (Ref 4, 5). The main advantage of the CSP use emanates from the nature of the energy source and mainly from its practical unlimited and non-polluting character. Nevertheless, its use is not yet applied in massive industrial production, mainly due to the fact that the solar power generation cannot be maintained constant during the daytime and the high cost of the relevant facilities.

As far as the welding technology is concerned, welding with concentrated solar energy has been attempted in the past, on three different alloys: aluminum alloys, titanium alloys, and steels. Karalis et al. (Ref 6) achieved the partial welding of 7075 aluminum alloy, triggering the experimentation on the CSE welding. Moreover, Romero et al. (Ref 7) achieved sound welds of tool steel and stainless steel plates of various thicknesses as well as welding of Ti-6Al-4V titanium alloy (Ref 8). In general, the obtained results of the CSE welding researches have demonstrated two important facts: Firstly, that alloys with high melting point and low heat conductivity (steels, titanium alloys) facilitate the welding procedure in comparison with metals with low melting point and high thermal conductivity like aluminum. Secondly, that the reduction in the solar beam area is essential, as it increases the power density and the penetration of the welding bead, while reduces the width of the weld metal area.

As far as the titanium alloy welding is concerned, it is mainly implemented by the use of industrial methods such as the gas tungsten arc welding (GTAW), the electron beam welding (EBW), and the laser welding (LW) techniques. The properties of titanium alloy welds have been investigated in terms of mechanical properties (Ref 9, 10) and microstructure (Ref 11-13) in several studies. Until now, most of the publications deal with the similar welding of pure titanium grades (Grade 1 to 4) and mainly with welding of Grade 5, which is the most widely used titanium alloy. Moreover, to the authors knowledge, the only investigation which concerns the CSE welding of titanium alloys has been carried out by Romero et al. who implemented and examined sound welds of Ti-6Al-4V plates of 5 mm in flush corner joint configuration (Ref 8), concluding that the weld with full penetration was obtained with a solar radiation of 1000 W/m^2 and a beam speed of 0.15 mm/s.

The current study aims to study the butt welding of titanium alloys sheets 1.3 mm thick with CSE. The main scientific innovation of the research concerns the examination of the mechanical properties of CSE weldments—which have not been under investigation until now—via the tensile testing of welded test pieces. More specifically, similar and dissimilar defect-free welds of Grade 4 and Grade 6 (Ti-5Al-2.5Sn) titanium alloys were achieved and examined. Grade 4 is recommended for applications which require improved corrosion resistance (Ref 14), while Grade 6 is characterized by good weldability and strength in elevated temperatures, and it is mainly used in the aerospace industry (Ref 15). Initially, the determination of the optimum conditions for the titanium alloy sheet welding was implemented and was subsequently followed by the examination of the microstructure, the microhardness distribution and the tensile properties of the CSE weldments.

D.I. Pantelis, M. Kazasidis, and **P.N. Karakizis**, Shipbuilding Technology Laboratory, School of Naval Architecture and Marine Engineering, National Technical University of Athens, 9 Heroon, Polytechniou St., Zografos, 157 80 Athens, Greece. Contact e-mails: pantelis@central.ntua.gr, marios_kazasidis@hotmail.com, and karakizisp@gmail.com.

2. Materials and Methods

2.1 Materials

The dimensions of the titanium alloy sheets were $100 \times 50 \times 1.3$ mm^3, and their typical chemical compositions (Ref 16) are presented in Table 1. The microhardness values of the base (unaffected) metals were determined, after several testing trials with the use of the Vickers hardness test method (HV 0.3) with a test force of 2.942 N and dwell time equal to 10 s.

The microstructures of the titanium Grade 4 and Grade 6 are presented in Fig. 1. Grade 4 consists entirely of almost uniform and polygonal equiaxed alpha grains (Fig. 1a) of the hexagonal close-packed (hcp) structure. Moreover, Grade 6 consists mainly of the equiaxed α phase (light phase) with a small amount of the body-centered cubic (bcc) ordered prior beta phase (dark phase) with the latter to be oriented along the rolling direction of the sheet as it is presented in Fig. 1(b) and as it is also mentioned by Yuri et al. (Ref 17).

2.2 Experimental Procedure

The experiments were performed by the use of a medium size solar furnace (MSSF) and a vertical concentrator of 1 kW thermal power on the focus point. Figure 2 presents schematically the track of the solar flux and the installation of the solar furnace. The solar radiation is reflected on the surface of a horizontal heliostat (Fig. 2a), passes through the shutters (Fig. 2b), and is subsequently collected on the vertical parabolic concentrator with a dish size of 1.5 m (Fig. 2c). Finally, it is concentrated on the circular focus point with a diameter of approximately 1 cm (Fig. 2d).

The welding processes were implemented inside a quartz chamber (Fig. 2d), which assures the maintenance of a shielding atmosphere. A vacuum pump was used in order to remove the atmospheric air from the interior of the chamber which was subsequently filled with argon of high purity (99%). The internal pressure was set at 1.5 bars. In the beginning, the edges of the titanium alloy sheets were subjected to grinding with a stainless-steel brush and further cleaning with acetone in order to remove the titanium oxide and dirt. Subsequently, the sheets were placed side by side on the aluminum clamping base in a butt weld joint configuration (Fig. 2d). The screws were tightened as an external constraint so that the deformation during the welding was minimized. Furthermore, the focus point of the solar beam was manually regulated to be on the top surface of the titanium sheets. The welding trials were performed along the largest dimension (100 mm), without the use of a filler material. The appropriate welding conditions which assure a sufficient penetration were determined with the following methodology: The main independent and controllable parameter was the welding speed, to wit, the velocity of the working table. The shutters were maintained fully opened and the welding trials were executed when the solar flux was approximately equal to 1000 W/m^2. The value of the welding speed in the initial trial was set at 4.9 mm/s and was gradually reduced until the penetration of the weld pool was found to be sufficient to assure a defect-free weld. After several bead-on-plate trials, it was concluded that the table speed must be equal to 2.2 mm/s for titanium alloys 1.3 mm thick and that this value is independent of the titanium grades under examination. The experimental data are presented in Table 2.

3. Results and Discussion

3.1 Macrostructural Analysis

After the welding procedure, the welds were examined macroscopically. Figure 3 presents the top surface of the as-

Table 1 Typical chemical compositions and the measured microhardness values of the used titanium alloys

	Chemical composition, wt.%									
	O	N	H	Fe	C	Sn	V	Al	Ti	Microhardness HV0.3
Grade 4	Max 0.4	Max 0.05	Max 0.015	Max 0.5	Max 0.1	…	…	…	Bal.	236
Grade 6	Max 0.2	…	…	Max 0.5	…	2.5	…	5	Bal.	346

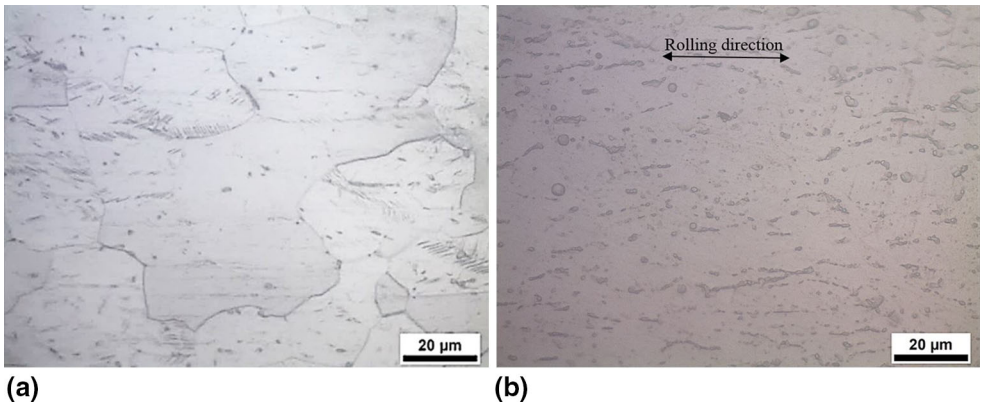

Fig. 1 Optical micrographs of the titanium alloys. (a) Grade 4 and (b) Grade 6

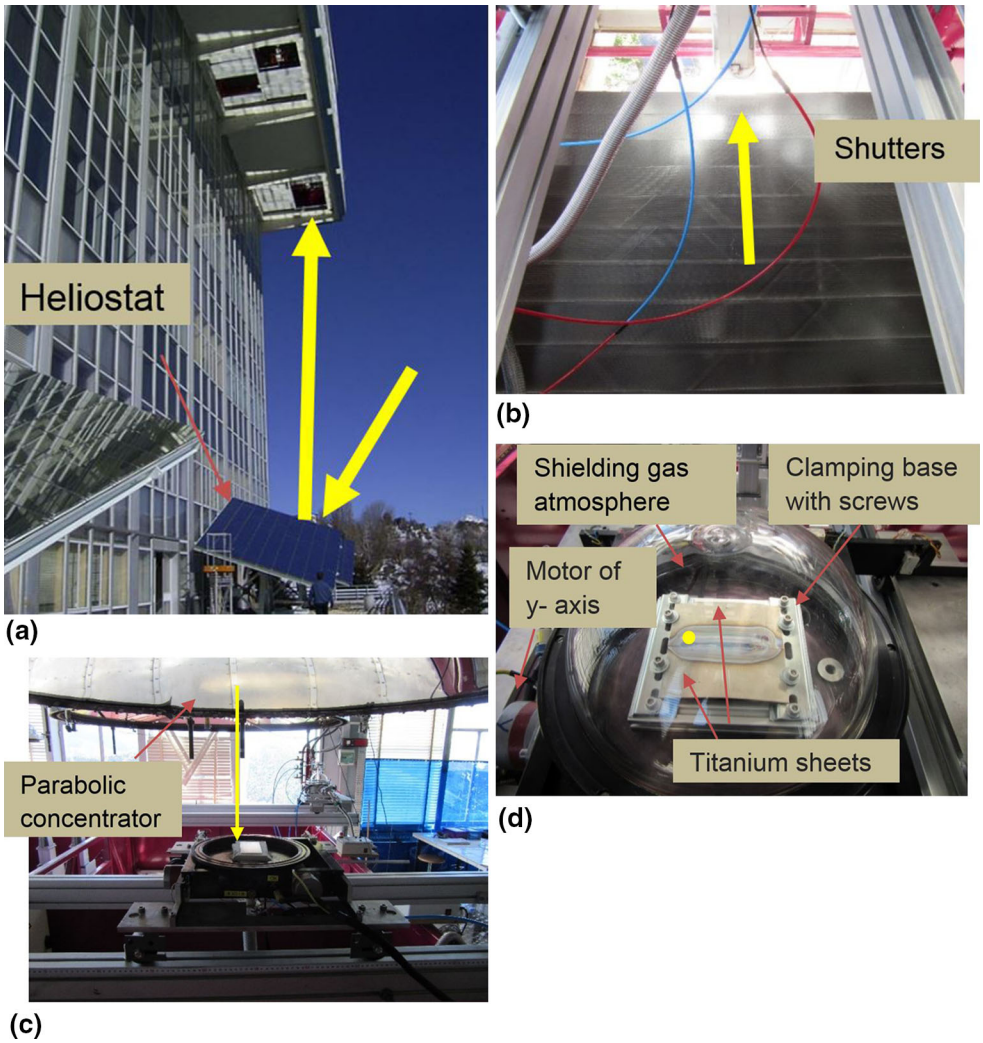

Fig. 2 Schematic view of the concentration system installation at the Solar Furnace in Font—Romeu (France). The yellow arrows indicate the path of the solar flux: (a) vertical reflection of the sun rays, (b) shutter opening control, (c) concentration of the radiation in the parabolic dish, and (d) concentration of the solar flux on the top surface of the titanium plates and the clamping set (Color figure online)

Table 2 Optimum experimental conditions of the defect-free welds

Titanium alloy	Weld method	Table speed, mm/s
Grade 4	Similar	2.2
Grade 6	Similar	2.2
Grade 4–Grade 6	Dissimilar	2.2

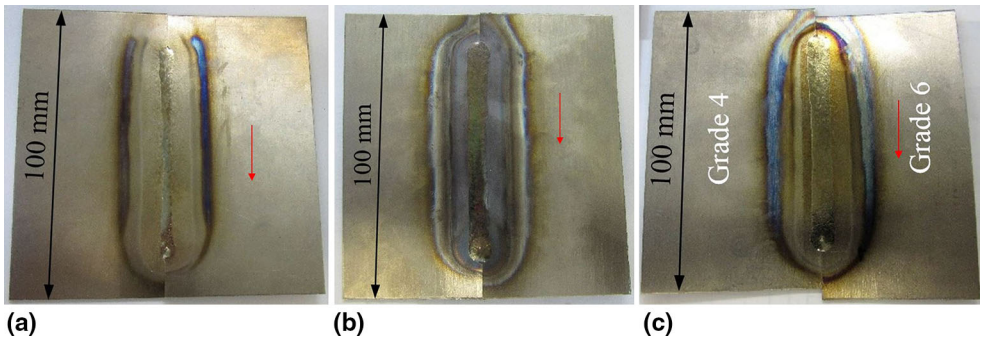

Fig. 3 Top surfaces of the as-received titanium alloy thin sheet welds: (a) similar weld of Grade 4, (b) similar weld of Grade 6, and (c) dissimilar weld between Grade 4 and Grade 6

received weldments, while the red arrows indicate the welding direction. It can be observed that the length of the beads did not extend to the edges of the sheets so that the possible melting of the aluminum clamping base (see Fig. 2d) was prevented. Furthermore, despite the fact that the sheets were clamped, a slight angular and bending distortion is evident. In addition, the width of the beads is almost uniform along the welding direction in all cases. It can be also observed that the weld bead of the similar weld of Grade 4 is narrower than in the other welds, due to the non-accurate adjustment of the solar beam on the top surface of the plates, as an automated focus regulation was not available.

On the other hand, a differentiation of the obtained surface coloration can be observed. In general, the titanium welds can

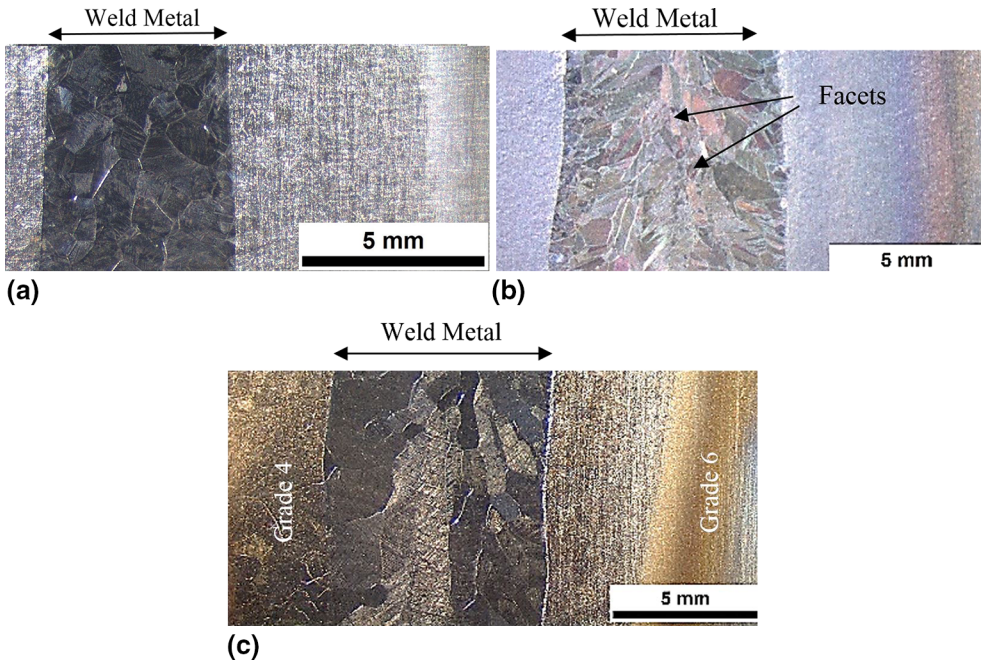

Fig. 4 Macrographs of the surface of the weld beads: (a) similar weld of Grade 4 alloy, (b) similar weld of Grade 6 alloy, and (c) dissimilar weld of Grade 4 and Grade 6

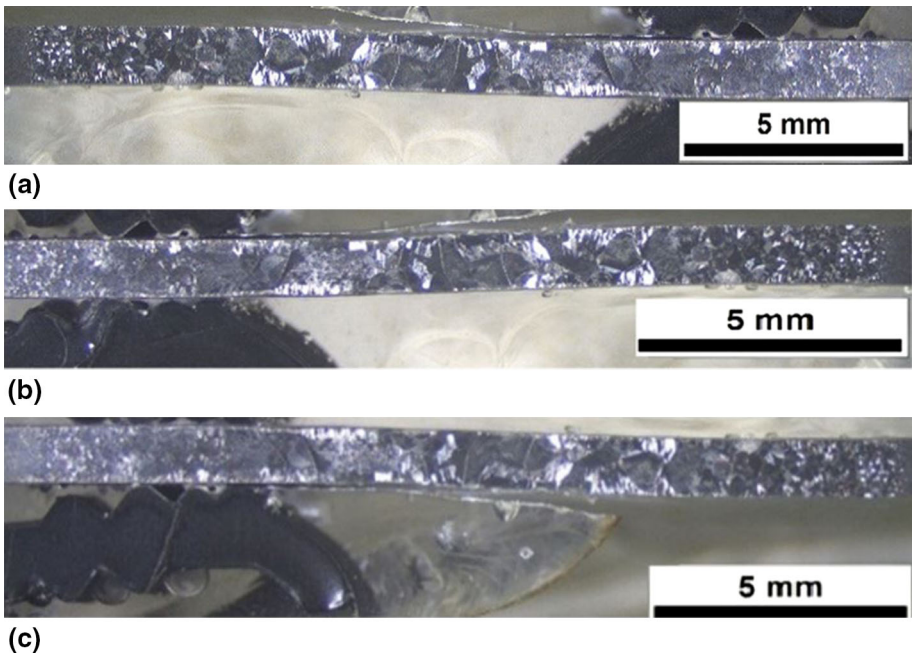

Fig. 5 Macrographs of the cross sections of the welds: (a) similar weld of Grade 4, (b) similar weld of Grade 6, and (c) dissimilar weld between Grade 4 and Grade 6

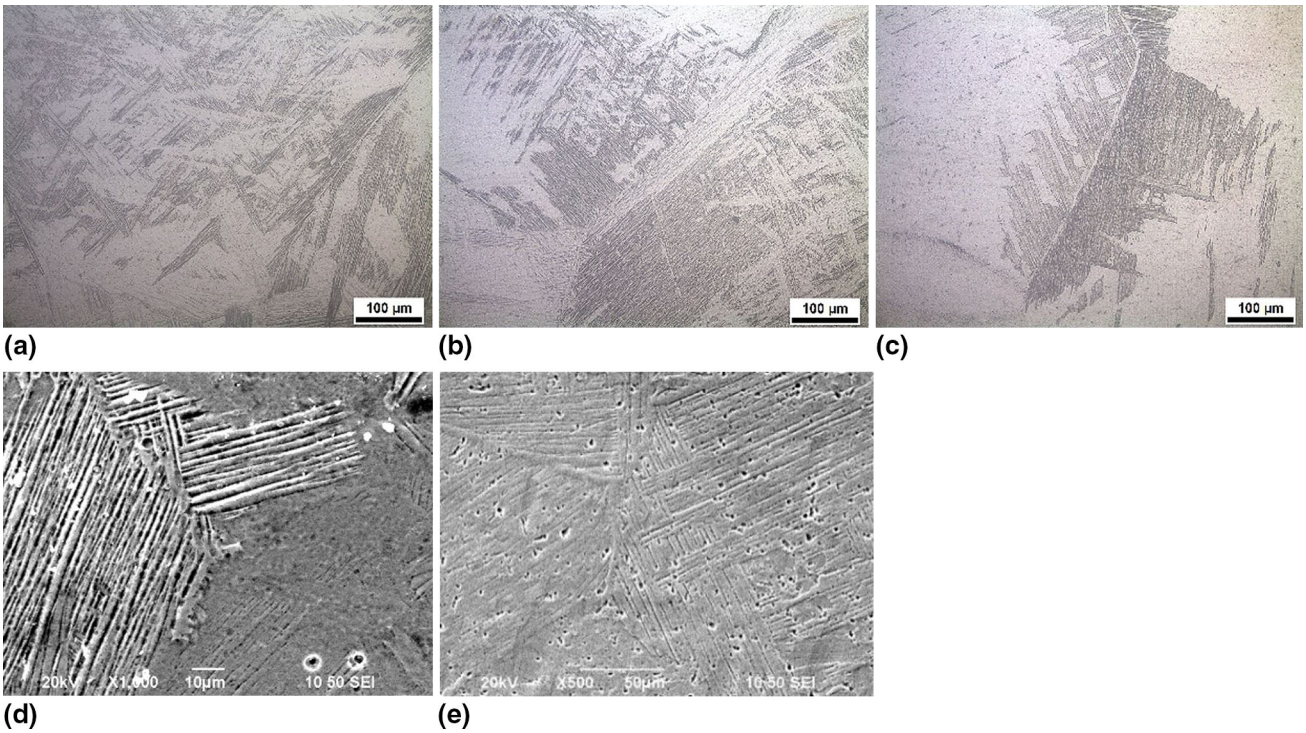

Fig. 6 Micrographs in the middle center of the weld metal areas: (a) optical micrograph of the similar Grade 4 weld, (b) optical micrograph of the similar Grade 6 weld, (c) optical micrograph of the dissimilar weld between Grade 4 and Grade 6, (d) electron micrograph of the similar Grade 6 weld, and (e) electron micrograph of the dissimilar weld between Grade 4 and Grade 6

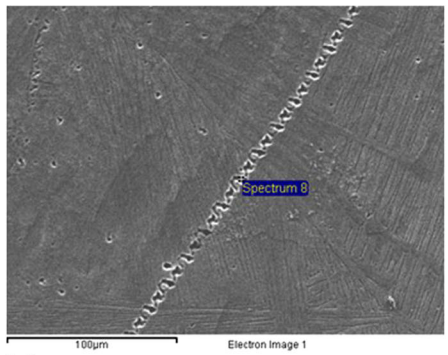

(a)

Element	Weight%	Atomic%
C K	1.60	6.06
Al K	1.00	1.69
Ti K	96.67	91.97
Sn L	0.74	0.28
Totals	100.00	

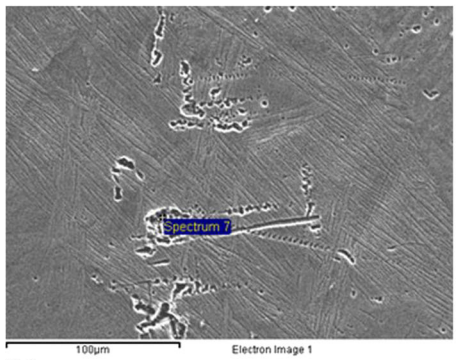

(b)

Element	Weight%	Atomic%
Al K	2.98	5.19
Ti K	96.18	94.47
Sn L	0.84	0.33
Totals	100.00	

Fig. 7 EDS micrographs and the chemical composition inside the fusion zone of the dissimilar welds (Grade 4–Grade 6): (a) linearly ordered particles and (b) randomly ordered particles

be classified, according to the color acceptance criteria depending on the observed oxidization (Ref 18, 19). More specifically, among the observed colors, the silver and the straw indicate low and medium oxidization, while the green and blue, higher. As presented in Fig. 3 and 4, the weld of Grade 4 is slightly oxidized (silver color), while the weld of Grade 6 is the most oxidized as it attains a mixed violet and green discoloration. The dissimilar weld (Grade 4–Grade 6) obtains a straw tint. The beads attain a smooth appearance and texture, while they present high symmetry. The weld pool facets are evident as can be observed in Fig. 4 and as they are indicatively pointed out with arrows in Fig. 4(b).

Subsequently, the test pieces were cut perpendicular to the welding direction, and their cross sections were subjected to grinding, polishing, and etching with the Kroll's reagent (100 ml H_2O, 6 ml HNO_3, 3 ml HF). The observation of the cross-sectional areas (see Fig. 5) indicated the absence of weld defects in macroscopic scale such as porosity, lack of penetration, and lack of fusion, while the boundaries between the weld metal and the HAZ could not be precisely determined macroscopically. Nevertheless, with the use of the Fig. 4 and of the hardness distribution profiles (as it is presented in paragraph 3.3), the mean width of the fusion zones and the heat affected zones was estimated at about 6.5 ± 0.7 mm and 3.3 ± 0.8 mm, respectively. Any obtained differentiation between the measured widths can be attributed to the variation of the thermal dissipation depending on the physical properties of each titanium alloy and to the manual adjustment of the focus on the top surface of the sheets. In addition, it can be stated that the width of the weld metal in all cases is lower than the diameter of the solar spot (lower than 10 mm) that can be attributed to the Gaussian-like spatial distribution (Ref 20) of the solar flux which is intense in the center of the spot and low near the circumference.

3.2 Microstructural Characterization

The microstructural characteristics inside the weld metal and the heat affected zone (HAZ) of all the welds were observed by the use of a light optical microscope and a scanning electron microscope and are presented as follows.

3.2.1 Weld Metal. Inside the fusion area, the predominant constituent is the Widmanstätten structure which is a characteristic basket weave pattern and is classified as a type of alpha phase (Fig. 6). It is formed by diffusion during the moderate cooling and its presence may reduce the ductility of structure, as stated by Askeland et al. (Ref 21). In addition, inside the fusion area, a small volume fraction of martensitic-type microstructure is observed (Fig. 6a and b).

In addition, the precipitation particles are observed in the similar weld of Grade 6 and in the dissimilar weld between Grade 4 and Grade 6. The study that follows focuses on the identification of the aforementioned phases. There are no significant changes in the morphology, the size, the color, and the shape of these phases between the different fusion zone areas. As a result, although a SEM-EDS study of the entire fusion zones was conducted, to avoid unnecessary repetition, the results that are going to be presented concern the center of the weld metal of the dissimilar weld.

The literature indicates that the precipitates may be the intermetallic compounds titanium aluminates (mainly Ti_3Al), which are products of eutectic reaction and embrittle the weld metal (Ref 22). As mentioned by Junaid et al. (Ref 23) and Wang et al. (Ref 24), in titanium grades which contain Sn and Al, such as the Grade 6, the formation of Ti_3Al is promoted. In

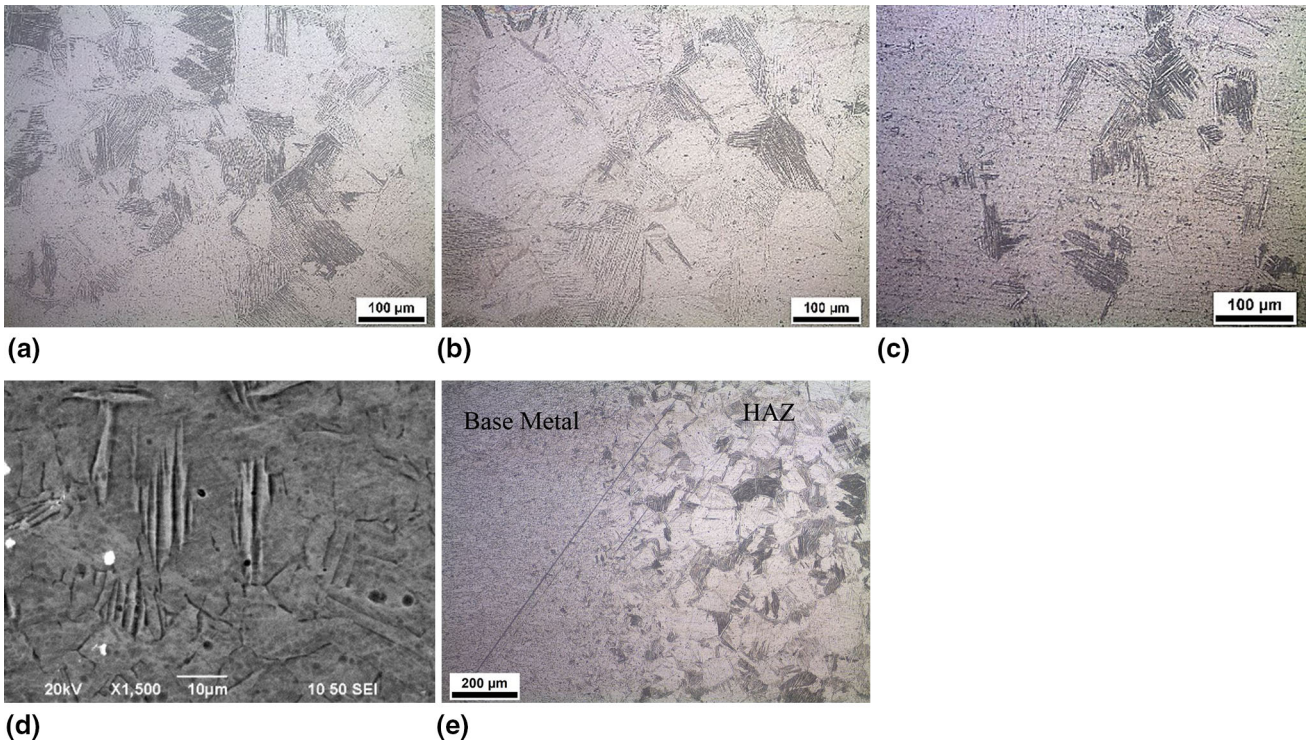

Fig. 8 Micrographs of the obtained HAZ microstructures: (a) optical micrograph of the Grade 4 weld, (b) optical micrograph of the Grade 6 weld, (c) optical micrograph in the dissimilar weld between Grade 4 and Grade 6 (side of Grade 6), (d) electron micrograph of the similar Grade 6 weld, and (e) transition area from the base metal to the HAZ in the Grade 4 weld

Fig. 7(a), linear ordered dispersion of such precipitates is presented. In contrast, a random order of these precipitation particles is depicted in Fig. 7(b).

Concequently, based on the aforementioned results, it can be mentioned that the observed precipitation particles are possibly titanium aluminides.

3.2.2 Heat Affected Zone. Inside the HAZ, the augmentation of the grain size is obvious (Fig. 8a, b and c) in comparison with the base metal (Fig. 1). This area is characterized by the nucleation of co-oriented alpha lamellae clusters inside the prior beta grain boundaries as it is depicted in Fig. 8(a), (b), and (c) and in Fig. 8(d) at a higher magnification. Moreover, Fig. 8(e) demonstrates indicatively the transition microstructure from the unaffected Grade 4 alloy to the heat affected zone.

3.3 Microhardness Distribution

The microhardness profiles of the specimens were determined with the use of the Vickers hardness test HV 0.3, which was carried out on the mid-thickness of the sheets. The distance between the measurements was 0.5 mm. Figure 9 depicts the hardness fluctuation through the principal distinct areas of the welds, viz. the weld metal, the heat affected zone, and the base metal.

Concerning the similar welds, the microhardness distribution curves indicate a significant augmentation inside the weld metal. More specifically, it is increased by approximately 20 and 16% in the similar welds of Grade 4 and Grade 6 compared to the respective hardness values of the base metals. The hardening of their structure inside the fusion zone can be attributed mainly to the low thickness of the sheets which results in faster cooling rates and thus to rapid solidification which promotes the formation of hard microstructures (Widmanstätten, martensite) as it was analyzed in the previous paragraph. In addition, in the dissimilar weld, the microhardness distribution follows a smooth transition from the softer (Grade 4) to the harder (Grade 6) titanium alloy. In this case, the hardness of the weld metal is between the respective values of Grade 4 and Grade 6. This phenomenon can be attributed to the higher dilution of the alloying elements inside the melted region as a result of the mixture of Grade 6 with the commercially pure titanium of Grade 4 and therefore the

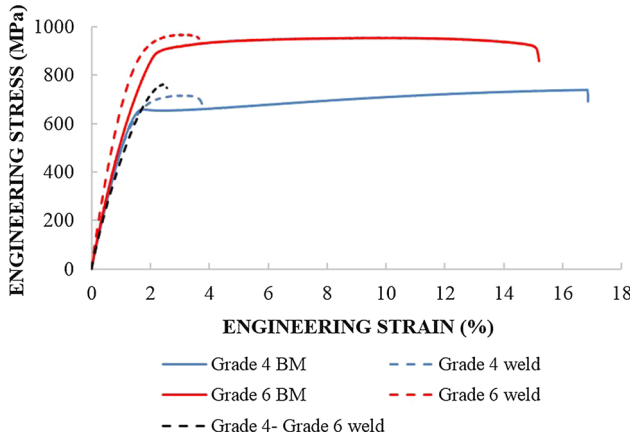

Fig. 10 Stress–strain curves of the welds and the base metals

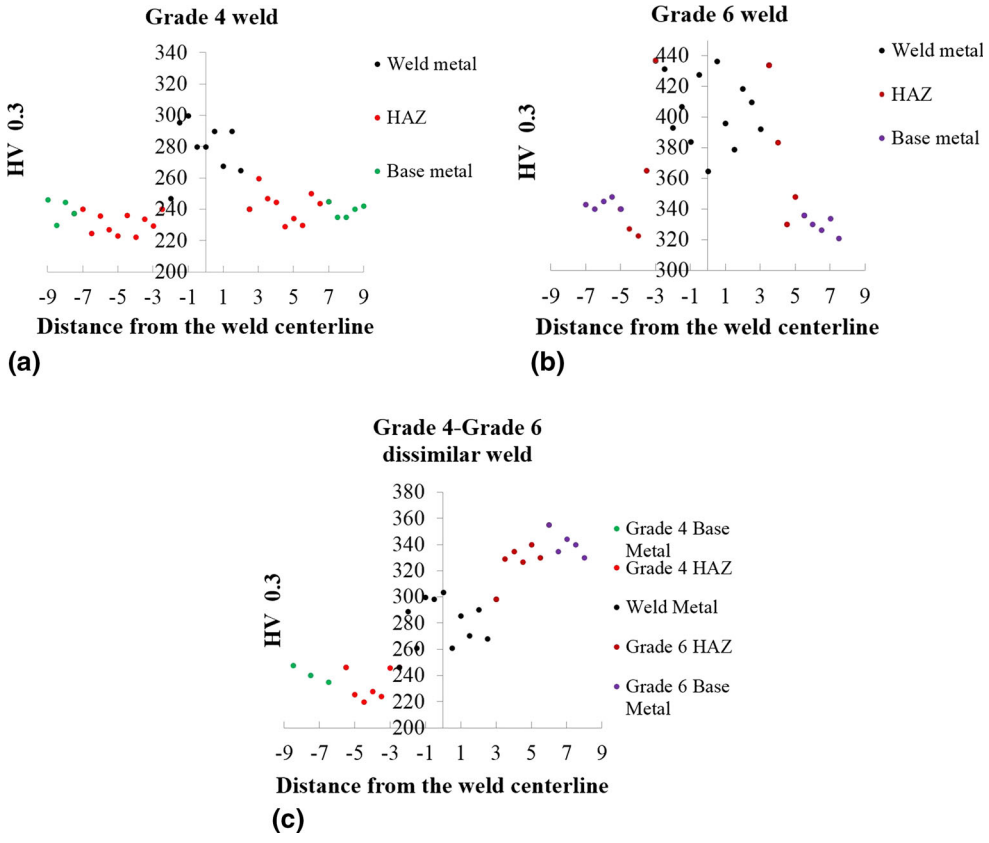

Fig. 9 Microhardness distribution of the welds: (a) Grade 4 similar weld, (b) Grade 6 similar weld, and (c) Grade 4–Grade 6 dissimilar weld

Table 3 Tensile properties of the welds and the base metals of the examined titanium alloys

Tensile properties	Grade 4 BM	Grade 6 BM	Grade 4 weld	Grade 6 weld	Grade 4–Grade 6 weld
Tensile strength, R_m, MPa	710	956	715	966	759
Yield strength, R_e 0.2%, MPa	661	907	663	897	716
Elongation after fracture, A, %	16.8	15.2	3.8	3.6	2.6

weakening of the solid solution strengthening mechanism which is of significant importance in the case of α titanium alloys, which contain Al and Sn (Ref 25). On the other hand, the hardness inside the heat affected zones in all cases is comparable to these of the base metals despite the increase of the grain size, that can be possibly attributed to the formation of the acicular alpha phase colonies.

It can be stated that the thickness of the plates and the welding technique have a major effect on the obtained hardness distribution. In relevant investigations on thick titanium plates, the maximum hardness is observed in the HAZ of gas tungsten arc welds of titanium Grade 2 (Ref 26). Moreover, in plates of titanium Grade 5 welded with the use of CSE, a moderate hardness distribution close to the base metal value was obtained into the different regions of the weld, mainly due to the low welding speed and the moderate cooling (Ref 8). On the other hand, Junaid et al. (Ref 23) mentioned that sheets of Ti-5Al-2.5Sn 1.6 mm thick, welded with LBW, demonstrated augmented microhardness values, inside the fusion zone at about 18% in comparison with the base metal. In addition, in EBW and GTAW of 0.5 thick pure titanium sheets, the fusion area was 14 and 28% harder than the base metal, respectively (Ref 27).

3.4 Tensile Testing

The weldments were further tested under uniaxial tensile loading, aiming to the estimation of the yield and the tensile strength, as well as the ductility of the weldments. The experiments were conducted on an MTS hydraulic testing machine, while the deformation speed was set equal to 0.25 mm/min. Due to dimensional restrictions derived from the small sheet size, custom-made coupons with rectangular cross section were extracted from each weld and from the base metal of both titanium grades, for comparison reasons. As a result, two tensile test pieces with dimensions $60 \times 15 \times 1.3$ mm^3 were machined for each case. The optimum stress–strain curves of each test are presented in Fig. 10.

The aggregate results can be also summarized in Table 3.

The tensile and the yield strength in the case of similar welds are approximately equal to the respective values of the base metal. Moreover, as far as the dissimilar weld is concerned, it attains R_m and R_e between the respective values of Grade 4 and Grade 6, but closer to these of Grade 4. On the other hand, the ductility as expressed from the elongation after fracture is tremendously reduced and it is about four times lower than the elongation of the base metal for the similar and the dissimilar weld. The welded specimens rupture slightly after the yield, while the fracture localization is observed inside the fusion area in all cases. The reason seems to be the existence of hard microstructural constituents and precipitates inside the fusion area. Comparatively to the above, in the similar welding of Grade 6 with LW and GTAW techniques and in the case of GTAW and EBW titanium alloy weld of high purity, the recorded R_m and R_e were close to the parent metal values (Ref 23) as it is also observed in the current study. Nevertheless, the elongation was equivalent to the base metal and the fracture localization was outside the weld metal in contrast to our experimental results.

4. Conclusions

In the present work, the feasibility of titanium alloys welding in the form of thin sheets by using concentrated solar energy was investigated. Similar welds of Grade 4 and Grade 6, as well as dissimilar weld between Grade 4 and Grade 6, were implemented and subsequently examined. The basic concluding remarks can be summarized as follows:

- In CSE welding of titanium alloys 1.3 mm thick, the table speed should be regulated at 2.2 mm/s when the solar radiation is at about 1000 W/m^2.
- Inside the weld metal, the predominant microstructural constituents are the Widmanstätten and the martensitic type. Linearly and randomly ordered, dispersed precipitation particles (probably Ti_3Al) are also observed.
- The microstructure of the heat affected zones consists of the acicular alpha phase inside the prior beta grain boundaries.
- The microhardness of the weld metal increases significantly in the similar welds of Grade 4 and Grade 6 in comparison with the base metal. In contrast, the fusion zone of the dissimilar weld attains a microhardness distribution between the respective values of Grade 4 and Grade 6.
- The welding process does not lead to a significant degradation of the yield and the tensile strength in similar welding, while the R_e and R_m of the dissimilar weld are approximately equal to the values of the titanium alloy of the lowest yield and tensile strength. On the other hand, in all cases the elongation is severely reduced due the embrittlement of the microstructure inside the fusion area.
- The major problem needed to be solved is the improvement of the microstructure inside the weld area in order to result in satisfactory ductility. This could be accomplished and examined in the framework of a future study by regulating and controlling the heat input and dissipation.

Acknowledgments

Financial support by the Access to Research Infrastructures activity in the 7th Framework Program of the EU (SFERA 2 Grant Agreement No. 312643) is gratefully acknowledged and the use of the facilities and its researchers/technology experts.

References

1. K. Yazawa, A. Shakouri, Material Optimization for Concentrated Solar Photovoltaic and Thermal Co-Generation. *InterPACK 2011, 6–8 July 2011, Portland, USA*. 2011, p. 1–7. https://doi.org/10.1115/IPACK2011-52190
2. H. Müller-Steinhagen and F. Trieb, Concentrating Solar Power: A Review of the Technology, *Ingenia*, 2004, **18**, p 43–50
3. P. Viebahn, Y. Lechon, and F. Trieb, The Potential Role of Concentrated Solar Power (CSP) in Africa and Europe—A Dynamic Assessment of Technology Development, Cost and Development and Life Cycle t Inventories Until 2050—The Potential Role of Concentrated Solar Power (CSP) in Africa, *Energy Policy*, 2011, **39**(8), p 4420–4430. https://doi.org/10.1016/j.enpol.2010.09.026
4. L.E.G. Cambronero, I. Cañadas, J.M. Ruiz-román, M. Cisneros, and F.A.C. Iglesias, *Journal of Materials Processing Technology Weld structure of joined aluminium foams with concentrated solar energy.*, 2014, **214**, p 2637–2643. https://doi.org/10.1016/j.jmatprotec.2014.05.032
5. I. García, M. Bayod, A. Conde et al., Concentrated Solar Energy Sintering Crossmark, *Mater Lett.*, 2016, **185**(August), p 420–423. https://doi.org/10.1016/j.matlet.2016.09.037
6. D.G. Karalis, D.I.Ã. Pantelis, and V.J. Papazoglou, On the Investigation of 7075 Aluminum Alloy Welding Using Concentrated Solar Energy, *Solar Energy Mater. Solar Cells*, 2005, **86**, p 145–163. https://doi.org/10.1016/j.solmat.2004.07.007
7. A. Romero and I. Garcı, *High melting point metals welding by concentrated solar energy.*, 2013, **95**, p 131–143. https://doi.org/10.1016/j.solener.2013.05.019
8. A. Romero, I. García, M.A. Arenas, V. López, and A. Vázquez, Journal of Materials Processing Technology Ti6Al4V Titanium Alloy Welded Using Concentrated Solar Energy, *J. Mater. Process Tech.*, 2015, **223**, p 284–291. https://doi.org/10.1016/j.jmatprotec.2015.04.015
9. S.M. Carvalho, C.A.R.P. Baptista, and M.S.F. Lima, Fatigue in Laser Welded Titanium Tubes Intended for Use in Aircraft Pneumatic Systems, *Int. J. Fatigue*, 2016, **90**, p 47–56. https://doi.org/10.1016/j.ijfatigue.2016.04.018
10. I. Uygur and I. Dogan, The Effect of TIG Welding on Microstructure and Mechanical Properties of a Butt-Joined-Unalloyed Titanium, *Metalurgija*, 2005, **44**, p 119–123
11. A.-M. El-Batahgy and T. Debroy, Nd-YAG Laser Beam and GTA Welding of Ti-6Al-4V Alloy, *Int. J. Eng. Tech. Res.*, 2014, **2**, p 43–50
12. N. Kashaev, V. Ventzke, V. Fomichev, F. Fomin, and S. Riekehr, Effect of Nd:YAG Laser Beam Welding on Weld Morphology and Mechanical Properties of Ti-6Al-4V Butt Joints and T-joints, *Opt. Lasers Eng.*, 2016, **86**, p 172–180. https://doi.org/10.1016/j.optlaseng.2016.06.004
13. S. Ferraris, S. Spriano, and G. Lorenzon, Intraoral Welding of Titanium Dental Implants: Characterization of the Joints, *J. Mater. Process. Technol.*, 2016, **235**, p 85–91. https://doi.org/10.1016/j.jmatprotec.2016.04.018
14. C. Leyens and M. Peters, *Titanium and Titanium Alloys: Fundamentals and Applications*, Wiley, London, 2003, https://doi.org/10.1002/9780470872864.ch61
15. ASM International Handbook V 2, Properties and Selection: Nonferrous Alloys and Special-Purpose Materials, *ASM Met. Handb.*, 1990, **2**, p 1300. https://doi.org/10.1016/S0026-0576(03)90166-8
16. ASM International. asm.matweb.com. http://asm.matweb.com/search/SpecificMaterial.asp?bassnum=mtu040
17. T. Yuri, Y. Ono, and T. Ogata, Effects of Surface Roughness and Notch on Fatigue Properties for Ti-5Al-2.5Sn ELI, Alloy at Cryogenic Temperatures, *Sci. Technol. Adv. Mater.*, 2003, **4**(4), p 291–299. https://doi.org/10.1016/S1468-6996(03)00058-5
18. ECSS, Space Product Assurance—Software Product Assurance. *Structure*, 1996, April, p. 1–25. ECSS-Q-ST-30-11C Rev 1
19. L. Jeffus, *Welding Principles and Applications*, Cengage Learning, Boston, 2011
20. B. Li, F.A.C. Oliveira, J. Rodríguez, J.C. Fernandes, and L.G. Rosa, Numerical and Experimental Study on Improving Temperature Uniformity of Solar Furnaces for Materials Processing, *Sol. Energy*, 2015, **115**, p 95–108. https://doi.org/10.1016/j.solener.2015.02.023
21. D. Askeland, P. Fulay, and W. Wright, *The Science and Engineering of Materials*, Nelson Education, Scarborough, 2010, https://doi.org/10.1016/0921-5107(92)90012-X
22. ASM, *Elements of Metallurgy and Engineering Alloys*, ASM, Materials Park, 2008
23. M. Junaid, M.N. Baig, M. Shamir, F.N. Khan, K. Rehman, and J. Haider, A Comparative Study of Pulsed Laser and Pulsed TIG Welding of Ti-5Al-2.5Sn Titanium Alloy Sheet, *J. Mater. Process. Technol.*, 2017, **242**(November), p 24–38. https://doi.org/10.1016/j.jmatprotec.2016.11.018
24. H. Wang, S. Wang, P. Gao, T. Jiang, X. Lu, and C. Li, Microstructure and Mechanical Properties of a Novel Near-α Titanium Alloy Ti6.0Al4.5Cr1.5Mn, *Mater. Sci. Eng. A*, 2016, **672**, p 170–174. https://doi.org/10.1016/j.msea.2016.06.083
25. G. Lutjering and J.C. Williams, *Titanium*, Springer, Berlin, 2007, https://doi.org/10.1007/978-3-540-71398-2
26. B.H. Choi and B.K. Choi, The Effect of Welding Conditions According to Mechanical Properties of Pure Titanium, *J. Mater. Process. Technol.*, 2008, **201**(1–3), p 526–530. https://doi.org/10.1016/j.jmatprotec.2007.11.164
27. Q. Yunlian, D. Ju, H. Quan, and Z. Liying, Electron Beam Welding, Laser Beam Welding and Gas Tungsten Arc Welding of Titanium Sheet, *Mater. Sci. Eng. A*, 2000, **280**(1), p 177–181. https://doi.org/10.1016/S0921-5093(99)00662-0